Contrib. Plasma Phys. 28 (1988) 1, 67–84

Discharge Development in ac Plasma Displays

J. RÖPCKE, R.-J. ZAHN

Akademie der Wissenschaften der DDR, Zentralinstitut für Elektronenphysik, Institutsteil Greifswald, Robert-Blum-Str. 8–10, Greifswald, 2200, DDR

Abstract

The discharge development in ac plasma displays is quantitatively assessed on the basis of comparatively great data quantities under well defined parameter conditions by means of computer controlled equipment. Investigated are ac plasma displays of three different sizes: PAF 58, 90 and PAF 128.

The development of an individual discharge in a stationary pulse sequence is described by analyzing the light emitted by the discharge and by comparing the data obtained with theoretical calculations.

Essential characteristics of the pulsed light emission of an ac plasma display discharge are the build-up time t_A, i.e. the period from cell voltage switch-on to the discharge maximum, and the characteristic time τ, which is the time constant describing the exponential growth of the discharge in its amplification range.

The theoretical model shows the transition, during discharge build up, from directionization of neon atoms, mainly at low τ values, to ionization essentially via the Penning effect at high τ values. Therefore the effective Townsend ionization coefficient is dependent on τ. The measured time constants of the discharge build up are in good agreement with the calculated values. Adaption between measurement and calculation is achieved by variation of the secondary emission coefficient γ of the cathode.

1. Introduction

The fundamental discovery leading to ac plasma display was made in 1964 by BITZER, SLOTTOW and WILLSON, who described discharges between insulated electrodes. The gas space in these cells is separated from the electrodes by a thin insulating layer. If the voltage applied to the electrodes is high enough, a formation of charge carriers by direct-ionization will occur in the gas space and the discharge process intensifies. The miniaturization of these discharge cells and their arrangement in a matrix with a high surface density has led to the opto-electronic module "ac plasma display" (Fig. 1).

The insulating layer of the electrodes is usually produced by thick film technique and covered with a MgO layer. The gas mixture used is Ne/Ar. Though the level of technological development of ac plasma displays is rather high further research is necessary to improve them.

Ac plasma displays have an inherent memory. The charged particles produced by the discharge voltage move to the insulating surfaces and are fixed there, thus becoming long lived wall charges. These charges act against the external field and erase the discharge. If the external discharge voltage applied to the electrodes is reversed, i.e. if an ac voltage

is used, the field generated by the wall charges has the same direction as the external field so that the subsequent discharge needs a lower external voltage for ignition.
The build up of discharges, the influence of wall charges and elementary processes occuring during ignition are investigated in this paper.

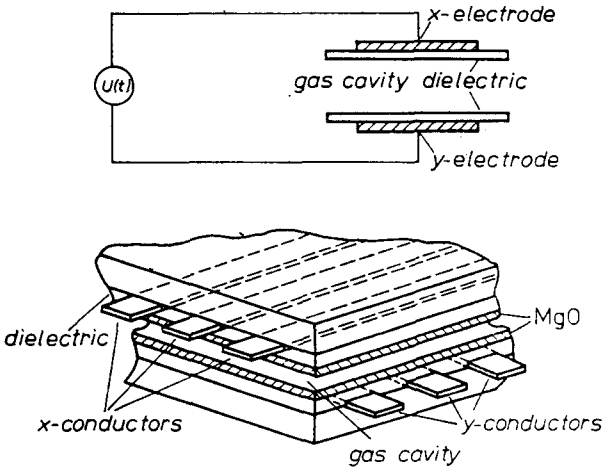

Fig. 1: Principle structure of a monochrome ac PDP and of a separate discharge cell

2. Measurement and Recording of Discharge Development

Discharge development was recorded by means of computer controlled equipment (Fig. 3). The light emitted by discharge passes through a microobjective and a light pipe into a multiplier (type M 12 FQC 51), whose exit signal goes into a box-car integrator. A nearly adequate reproduction of the time-dependent light emission of the individual discharge is possible by a high scanning frequency of the box-car integrator. The build-up time t_A is indicated by the position of the maximum (Fig. 2). The logarithmic presentation permits to determine the characteristic time τ, which is the time constant of discharge development in the amplification range.

The sustainer used has some particularities in its pulse regime (Fig. 4). The pulse heights U_1, U_2 and U_3 can be adjusted separately. U_1 is the sustain pulse voltage which

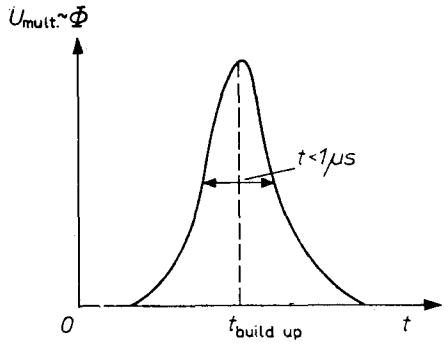

Fig. 2: Principle form of the light emission of an ac PDP discharge

produces a reproducible transitional state. U_2 is the erase pulse voltage which leads to a minimization of the wall voltage, ideally to a zero voltage, U_3 is the measuring pulse voltage, for which there is a gap of about 70 μs in which it can be shifted in steps of 2.5 μs. Therefore the possibility is given to vary in a wide range the conditions for the discharge build up by a single pulse, the pulse duration being 10 μs.

The measurements were made on ac plasma displays of three different sizes, PAF 58, PAF 90 and PAF 128 (PAF means **P**lasma-**A**nzeige-**F**eld, the number corresponds to number of x- and y-conductors). The thickness of the gas space was approximately 0.14 mm, the thickness of the insulating layer being about 10 μm and of the MgO overcoat

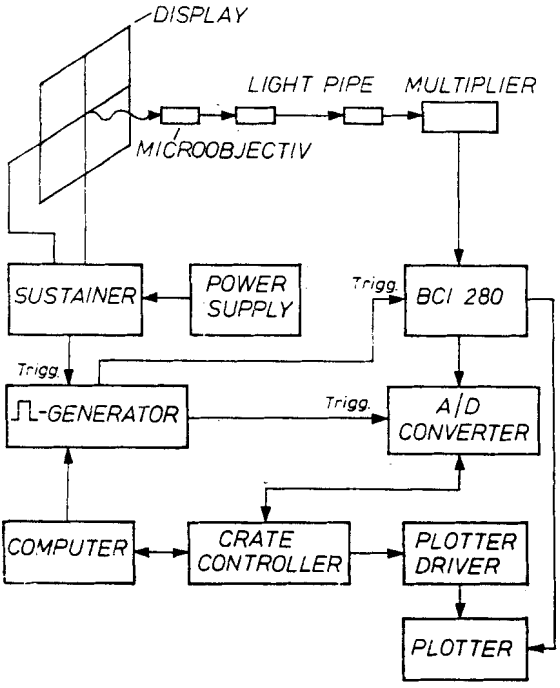

Fig. 3: Experimental equipment

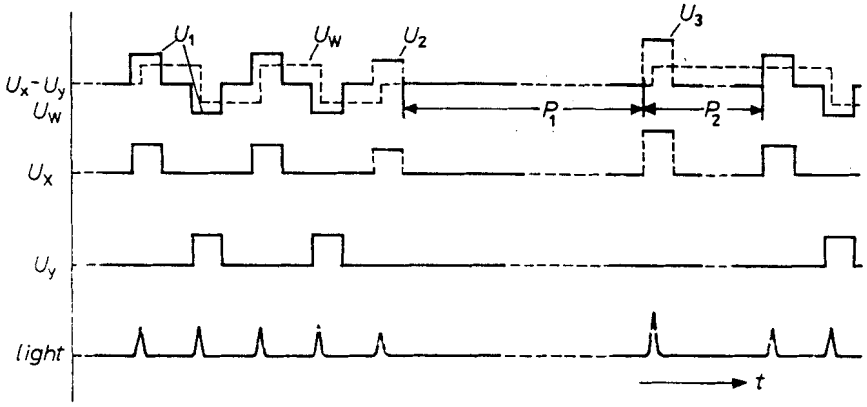

Fig. 4: Pulse regime of the sustainer

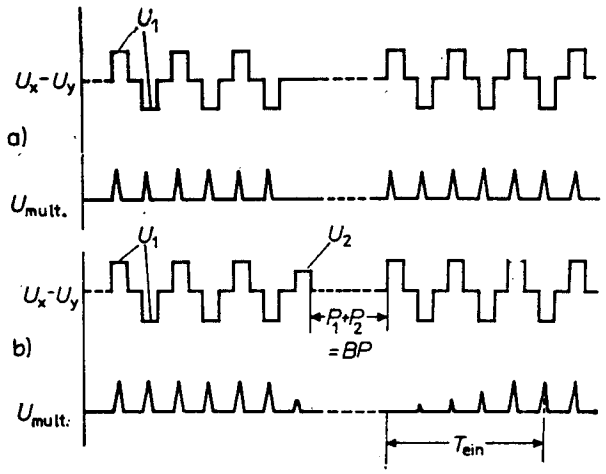

Fig. 5: Used pulse regimes

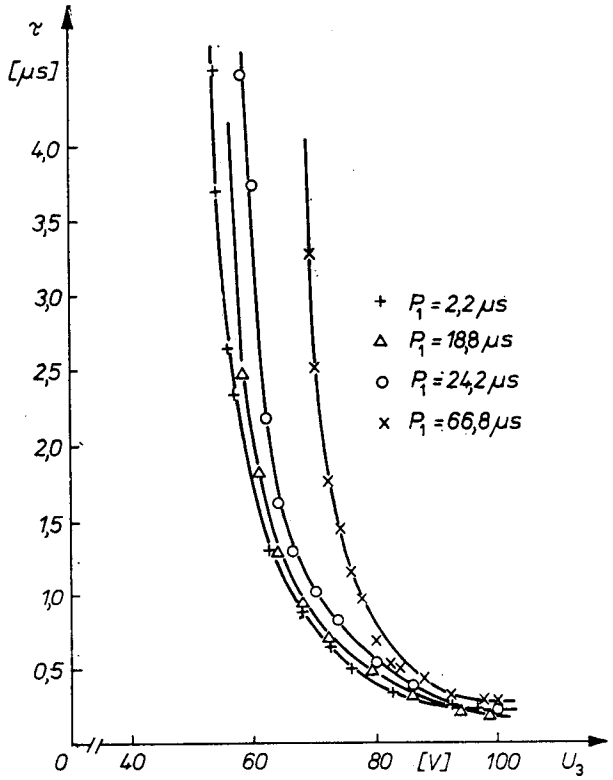

Fig. 6: Dependence of the characteristic time τ on the measuring pulse voltage U_3 Parameter: P_1, — PAF 58 —

material about 100—200 nm. The gas used was a mixture of neon with 0.1% argon at a pressure of 53 kPa (400 Torr). In PAF 58 the dot distance is 1 mm and the electrode breadth 0.35 mm. For PAF 90/128 these values are 0.8 mm dot distance and 0.2 mm electrode breadth.

The investigations were made using two different pulse regimes (see Fig. 5):

1. Without using an erase pulse ($U_2 = 0$V), i.e. with no external influence on plasma and wall voltage before the measuring pulse (Fig. 5a).
2. By applying an erase pulse so that plasma and wall voltage can be varied before the measuring pulse (Fig. 5b). The amplitude of the erase pulse (U_2) is adjusted in such a way that the period (T_{ein}) of the following discharge is as long as possible. This is the state in which, using suitable erase pulse voltage, we find a maximum of wall charge reduction and also a maximum of deionization processes in the plasma.

3. Measurements without Using an Erase Pulse

Fig. 6 shows measurements made on ac plasma displays PAF 58 without using an erase pulse (Fig. 5a). The cell ignites if the discharge voltage reaches the value of 108 V for U_1 and extinguishes at $U_1 = 80$ V. The dependence of the characteristic time τ on measuring pulse voltage is shown, the parameter being the delay time P_1. With decreasing $U_3\tau$ becomes larger and approaches infinity. This U_3 limit is 56 V for $P_1 = 2.2\ \mu$s and increases for $P_1 = 66.8\ \mu$s to about 68 V.

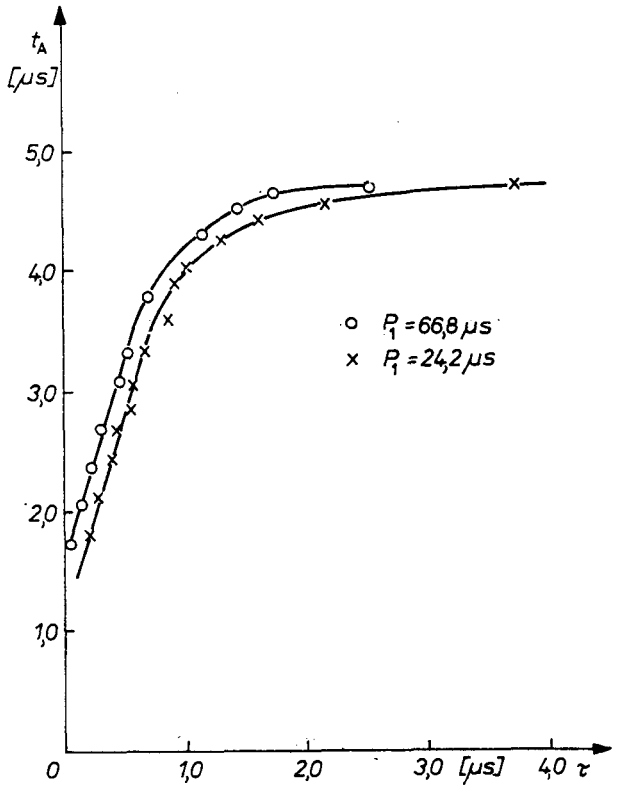

Fig. 7: Dependence of the build-up time t_A on the characteristic time τ
Parameter: P_1, — PAF 58 —

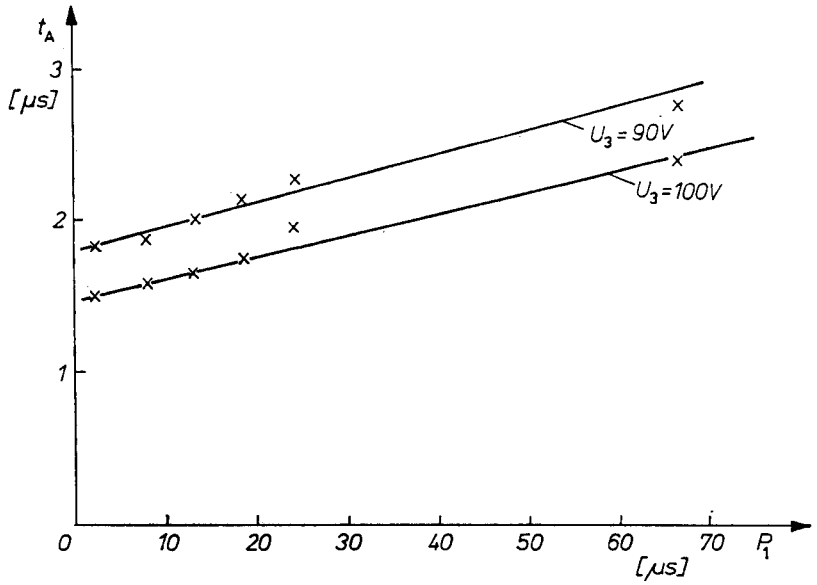

Fig. 8: Dependence of the build-up time t_A on the delay time P_1
Parameter: U_3, — PAF 58 —

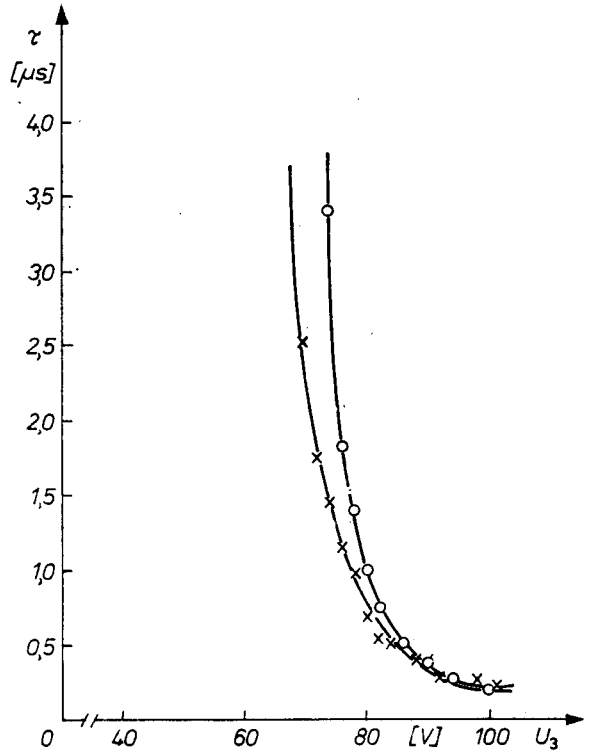

Fig. 9: Dependence of the characteristic time τ on the measuring pulse voltage U_3
(The display electrodes were changed.) — PAF 58 —

This increase of the U_3 limits with growing P_1 reflects the time-dependent deionization of the plasma as well the wall charge reduction.

NASTASE and co-workers [26] reported average deionization times for Ne-Ar-mixtures under ac plasma display conditions (Ne + 0.1% Ar, 400 Torr, square-wave voltage) of 4.5 μs, which is in good agreement with values known from the literature [27].

Fig. 7 indicates a linear relationship between build-up time t_A and characteristic time τ up to $\tau \approx 1$ μs, making evident the role of delay time as a parameter under these conditions. For same characteristic times the build-up time of the discharge is higher even if the delay times are increased. Using a similar method of measurement and nearly the

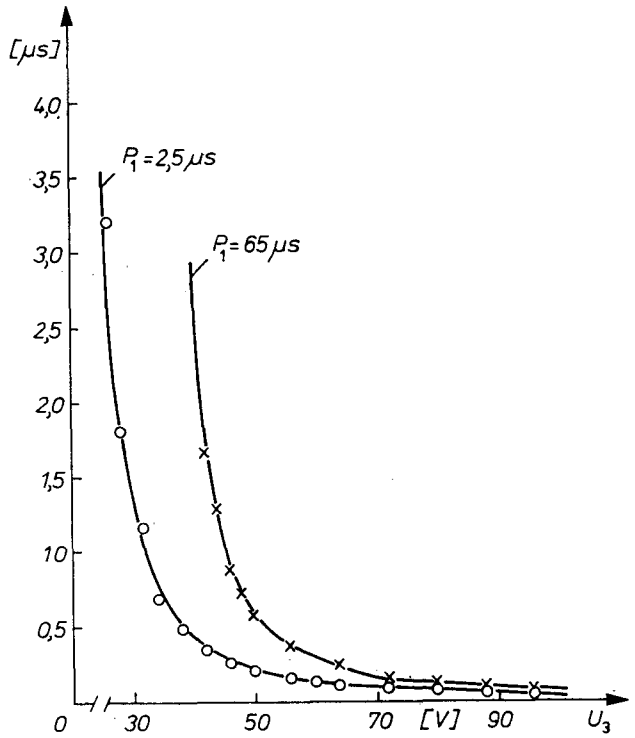

Fig. 10: Dependence of the characteristic time τ on the measuring pulse voltage U_3 Parameter: P_1, — PAF 90 —

same pulse regime ANDOH and co-workers obtained for MgO covered electrodes maximum build-up times of about 4 μs [24]. Short build-up times averaging 2—3 μs are ascribed to such MgO layers, because they have a relatively high effective secondary emission coefficient γ_{eff} in Ne-Ar-mixtures.

Fig. 8 shows the dependence of the pulse discharge build-up time on delay time, the measuring voltage U_3 being the parameter. The monotonous growth of the build-up time with delay is evident.

Figs. 10 and 11 show results of measurements under the same conditions for a display cell of PAF 90. Here the voltage U_1, at which the cell ignites, is 101 V and a voltage of 76 V is needed for quenching. The limits for U_3 are in the range of 25—40 V, depending on delay P_1, as compared to the 55—70 V of PAF 58. This suggests an appreciably improved effective secondary emission coefficient of the PAF 90 MgO layer. Moreover,

dispersion of the measured values of characteristic time and build-up time is considerably diminished. ANDOH and co-workers related the diminished dispersion of the build-up time values to an improved quality of the MgO layer [24].

The measured values shown in Fig. 9 suggest different properties of the plate surfaces of the PAF 58 we used. The measurement conditions remained largely the same, only the display electrodes were changed between the two experiments. The result is a clearly different graph of the dependence of the characteristic time on the measuring pulse

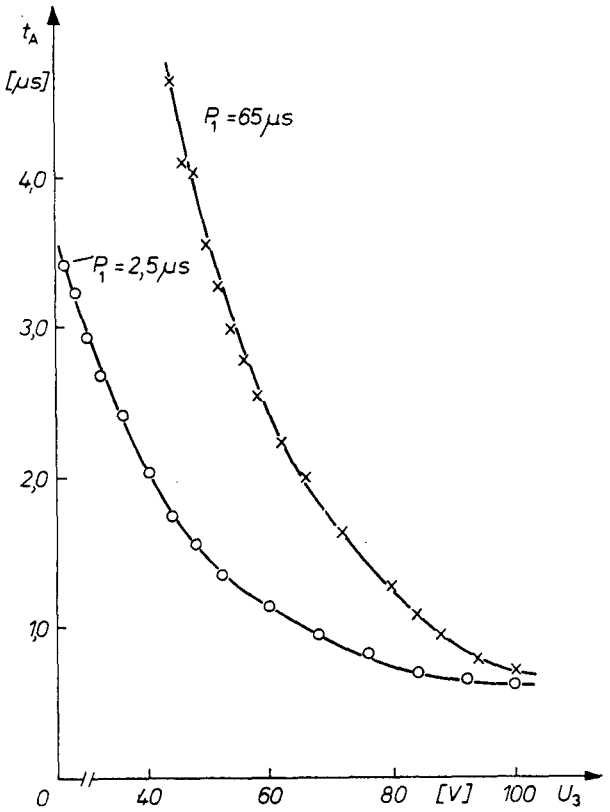

Fig. 11: Dependence of the build-up time t_A on the measuring pulse voltage U_3
Parameter: P_1, — PAF 90 —

voltage. The U_3 limits differ by 6 V. The graph with the increased U_3 limits points to a decreased effective secondary emission coefficient of the MgO layer.

The possibility to calculate the secondary emission coefficients of MgO layers directly from statically measured breakdown voltages is described in the literature (e.g. [28]). However, this calculation has to be based on the Townsend discharge theory. This theory provides a well-defined relationship between the secondary emission coefficient γ and the breakdown voltage U_z.

$$\gamma = \frac{1}{\exp\left[\eta(U_z - U_0)\right] - 1}$$

η — ionization function
U_0 — voltage leading to an equilibrium state in the discharge.

But when using the tabulated ionization function $\eta\,(E/p)$ we have to assume homogeneous fields and a quasi-stationary ignition process. Therefore, breakdown voltage measurements are done, e.g. on model discharges, using substantially decreased frequencies ($f/p = 5-10$ Hz/Torr) and sinusoidal waves. To apply the results obtained in model discharges to displays, additional assumptions about the validity of similarity principles are necessary.

The main ionization process in ac plasma displays is the two-stage Penning process. For this reason the ionization function η should be used dynamically.

4. Measurements by Means of an Erase Pulse

For assessing ac PDP cell properties on the basis of their discharge behaviour the magnitude of the wall charge has to be taken into account. If the electrical capacity of the discharge cell is known, the wall charge can be calculated from the wall voltage. In the literature there have been detailed discussions on the possibility to measure the wall voltage by using discharge current integration and by charge transfer curves [1—4, 16].

If an erase pulse is used in the dynamical pulse regime the display cell shows a modified wall charge. By suitable choice of the erase pulse voltage U_2 (pulse regime Fig. 5b) the wall charge and thus the wall voltage in the discharge cell before the measuring pulse can be minimized. For the minimum wall charge, ideally it becomes zero, the measuring

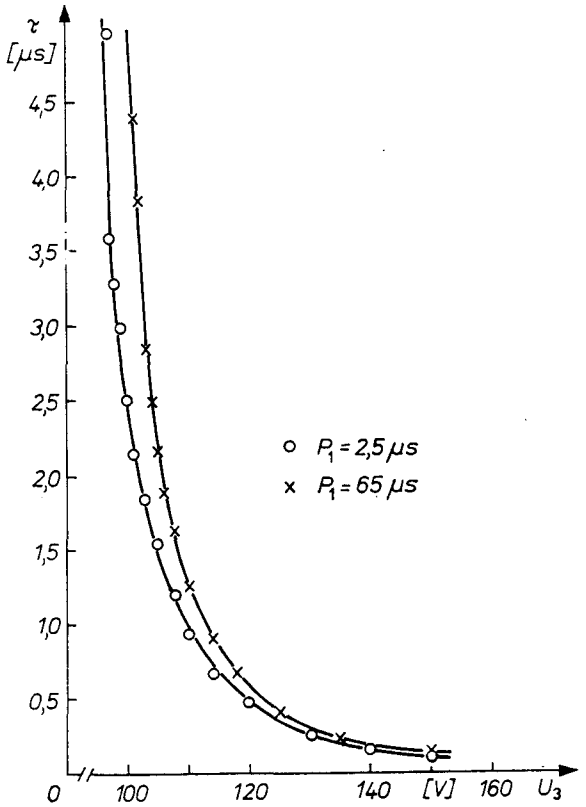

Fig. 12: Dependence of the characteristic time τ on the measuring pulse voltage U_3 Parameter: P_1, — PAF 90 —

pulse voltage U_3 coincides with the cell voltage. The discharge activity caused by the measuring pulse can be regarded, in good approximation, as a new ignition which is wall voltage independent. This technique leads to a good reproducibility of the measuring conditions at high recurrence frequency and was already proposed by ANDOH [24]. It is similar to the method used by UCHIIKE and co-workers for investigating the interaction between erase pulse and electron and ion concentration in the discharge cell [18].

Fig. 12 shows the dependence of the characteristic time τ on the measuring pulse voltage U_3 if an erase pulse ($U_2 = 49{,}5$ V) is used in the sustainer pulse regime. The measurement was done on a PAF 90 discharge cell. The delay times were 2.5 µs and 65 µs,

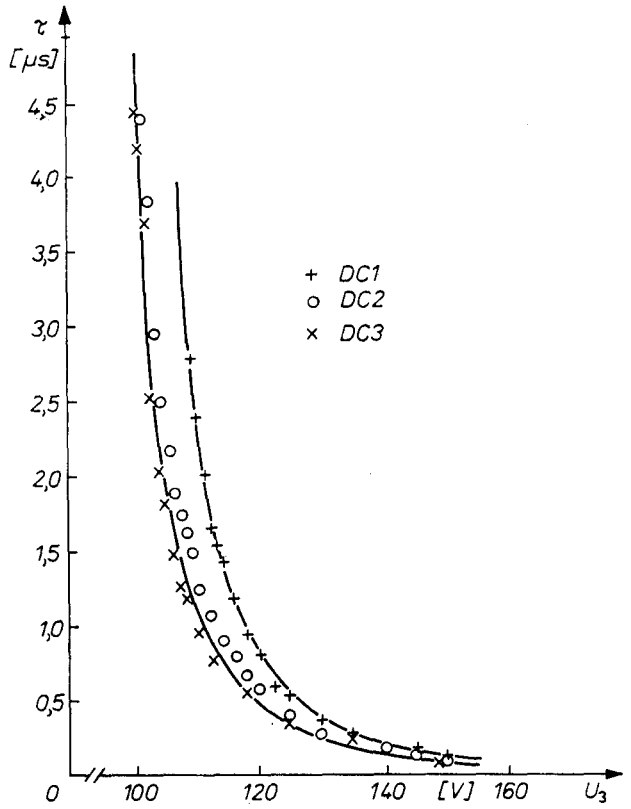

Fig. 13: Dependence of the characteristic time τ on the measuring pulse voltage U_3 of three PAF 90 discharge cells

which again clearly shows the U_3 limit dependence on delay time, the U_3 limit for $P_1 = 2.5$ µs being 96 V and for $P_1 = 65$ µs 100 V. The comparable measurement without wall voltage minimization produces, for varying delay times, a difference of about 15 V. This illustrates the effects of an erase pulse i.e. quick deionization of the plasma and wall charge reduction. The relatively small difference of the U_3 limits shows (Fig. 12) that after occurrence of a discharge activity caused by a suitable erase pulse deionization and wall charge reduction process have, for the most part, terminated within some µs. UCHIIKE and co-workers calculated that the wall charge in a display cell decreases after a suitable erase pulse of 10 µs to 1/10 (10^{-9} C/cm^2) of its maximum value. Electron and ion density are only about $0.3 \cdot 10^{12}$ cm^{-3} (maximum $2.4 \cdot 10^{12}$ cm^{-3}) after 10 µs. These

values refer to the discharge space. At the electrodes the charge carrier density approaches zero [17]. After an erase pulse and the related discharge the discharge space can be assumed to be nearly fieldfree. The decay of the remaining plasma is then effected by ambipolar diffusion and electron ion recombination.

WEBER describes the role of these elementary processes in connection with life time investigations on relative long lived plasmas [4, 29].

MÜLLER and ZAHN arrived at similar conclusions [25]. The basis for an explanation of positive and negative charges on insulators is provided by an appropriate band model of

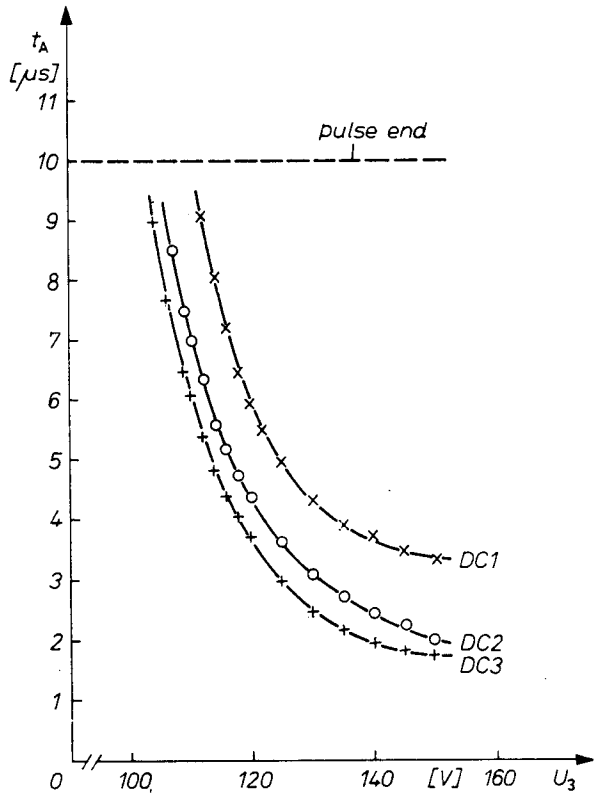

Fig. 14: Dependence of the build-up time t_A on the measuring pulse voltage U_3 of three PAF 90 discharge cells

the solid. With regard to MgO a detailed explanation is given by ABOELFOTOH and co-workers [19—23, 35].

The build-up of a negative wall charge can be seen as a result of electron capture in traps of the insulator, for example MgO. Positive charges result from electron release from the solid by positive ions and metastable atoms via Auger neutralization or Auger de-excitation process [9—14]. If an ac plasma display cell works with square wave pulses, a permanent charge exchange of the MgO layers occurs. The neutralization of positive charges is the result of slow electron capture from the discharge space. Negative charges are reduced by Auger detachment process. These complex interactions are reflected in the value of the effective secondary emission coefficient. If this model is used, a suitable

chosen erase pulse amplitude causes such a discharge in the cell, which produces just as many charged particles (ions, electrons) and excited atoms as are needed to neutralize the wall charges by the described mechanisms. Due to the relative low erase pulse voltage no more plasma components are available for a new wall charge build-up. At the end of the erase pulse the discharge cell is nearly fieldfree and has only a comparatively small remaining plasma. If now a new discharge is to be ignited, a relatively high voltage is necessary (i.e. 150 V).

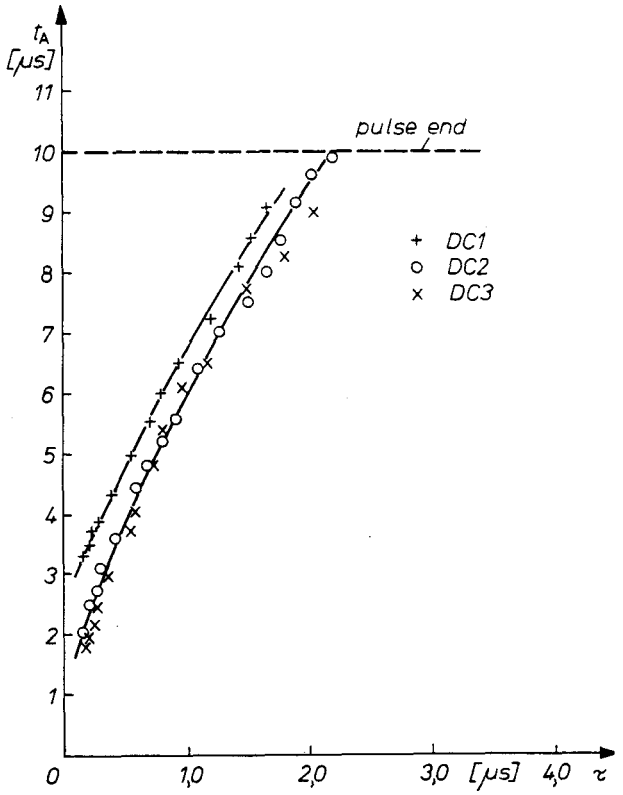

Fig. 15: Relationship between build-up time and characteristic time of three PAF 90 discharge cells

The build-up times of discharges after an erase pulse (Fig. 14) considerably exceed those of the undisturbed state (Fig. 11). With decreasing discharge voltage there is a particularly strong increase of the build-up times, which are limited by the duration of the square wave pulses (10 µs). Fig. 15 shows the relationship between build-up time and characteristic time of three PAF 90 discharge cells. The measured values show a good linear relationship between t_A and τ. Different effective secondary emission coefficients of the discharge cells lead to a parallel displacement of the straight lines. The PAF 128 produced largely the same experimental results as the PAF 90 discharge cells. As expected, the measured values and their physical interpretation are not directly related to the size of the display.

5. Calculation of the Charakteristic Time and Comparison with Experimental Results

The fundamental concepts of the time-dependent discharge build-up in low pressure glow discharge are based on the Townsend mechanism. Already in 1930 STEENBECK succesfully calculated the build-up time of glow discharges [32]. Under simplifying assumptions and by consideration of the ion flight time between anode and cathode SCHADE obtained experimentally reproducible discharge build-up results in rare gases [30].

Starting from the carrier balance equation for ions and electrons BARTHOLOMEYCZYK considered wall diffusion and photo-ionization and derived formulae for breakdown condition and build-up time [5]. Also starting from electron and ion balance equations other authors estabilished the build-up times of low current low pressure discharges in pure rare gases and in rare gas mixtures [6, 7, 33]. Still others investigated serveral interaction mechanisms of ions and metastable atoms with the cathode [8, 31].

The theoretical interpretation of the time-dependent discharge build-up in ac plasma displays takes into account the plasma physical phenomena and also the influence of the solid surfaces surrounding the discharge area. The displays were filled with neon argon Penning mixtures. Therefore the theoretical model has to include, in addition to directionization of gas atoms, the Penning ionization of argon by metastable neon atoms. Thus, in contrast to [5, 32, 33], the output equation system needs to be enlarged. The equation system (1)—(4) balances electrons, Ne^+ and Ar^+ ions and metastable neon atoms alike.

$$\frac{\partial}{\partial t}\left(\frac{j_-}{v_-}\right) = -\frac{\partial}{\partial x} j_- + \alpha j_- + n_a \cdot n_g \cdot z_p \cdot p \cdot x \tag{1}$$

$$\frac{\partial}{\partial t}\left(\frac{j_+^{Ar}}{v_+^{Ar}}\right) = \frac{\partial}{\partial x} j_+^{Ar} + n_a \cdot n_g \cdot z_p \cdot p \cdot x \tag{2}$$

$$\frac{\partial}{\partial t}\left(\frac{j_+^{Ne}}{v_+^{Ne}}\right) = \frac{\partial}{\partial x} j_+^{Ne} + \alpha j_- \tag{3}$$

$$\frac{\partial}{\partial t} n_a = \varepsilon j_- - n_a \cdot n_g \cdot z_p \cdot p \cdot x \tag{4}$$

n_a — concentration of metastable Ne atoms
n_g — concentration of Ne atoms in ground state
z_p — Penning collision rate
p — pressure
x — mixture proportion
α — number of Ne^+ ions produced by one electron per cm
ε — number of metastable Ne atoms produced by one electron per cm
j_-, j_+^{Ne}, j_+^{Ar} — particle flux density of electrons, Ne^+ and Ar^+ ions
v_-, v_+^{Ne}, v_+^{Ar} — velocity of electrons, Ne^+ and Ar^+ ions.

The equation system (1)—(4) can be solved using a separation ansatz developed by BARTHOLOMEYCZYK so that a separate calculation of space and time dependence with the help of the boundary conditions (5) and (6) is possible.

$$j_-(0) = \gamma^{Ar} \cdot j_+^{Ar}(0) + \gamma^{Ne} \cdot j_+^{Ne}(0) \quad \text{— at the cathode} \tag{5}$$

$$j_+(d) = j_+^{Ar}(d) = j_+^{Ne}(d) = 0 \quad \text{— at the anode.} \tag{6}$$

The secondary emission coefficients for Ne^+ and Ar^+ ions γ^{Ne} and γ^{Ar} are material constants of the MgO layer. The solution leads to two equations (7) and (8), from which the characteristic time τ can be calculated interactively.

$$\frac{\varepsilon \cdot \tau}{\tau + \tau_{met}} \frac{\exp\left[\left(\alpha_{eff} - \frac{1}{v_{Ar} \cdot \tau}\right) \cdot d\right] - 1}{\alpha_{eff} - \frac{1}{v_{Ar} \cdot \tau}} = \frac{\delta}{\delta \cdot \gamma^{Ar} + (1 - \delta)\gamma^{Ne}} \tag{7}$$

$$\alpha \frac{\exp\left[\left(\alpha_{eff} - \frac{1}{v_{Ne} \cdot \tau}\right) \cdot d\right] - 1}{\alpha_{eff} - \frac{1}{v_{Ne} \cdot \tau}} = \frac{1 - \delta}{\delta\gamma^{Ar} + (1 - \delta)\gamma^{Ne}} \tag{8}$$

δ — portion of argon ion current of the whole ion current hitting the cathode
τ_{met} is the lifetime of metastable Ne atoms:

$$\frac{1}{\tau_{met}} = n_g \cdot z_p \cdot p \cdot x$$

$$\alpha_{eff} = \alpha + \frac{\varepsilon \cdot \tau}{\tau + \tau_{met}}$$

$$\frac{1}{v_{Ar}} = \frac{1}{v_-} + \frac{1}{v_+^{Ar}}, \quad \frac{1}{v_{Ne}} = \frac{1}{v_-} + \frac{1}{v_+^{Ne}}$$

are the harmonic means of carrier velocities.

Equations (7) and (8) contain an effective Townsend ionization coefficient. α_{eff} represents the number of ions and electrons produced per cm as a result of direct and Penning ionization.

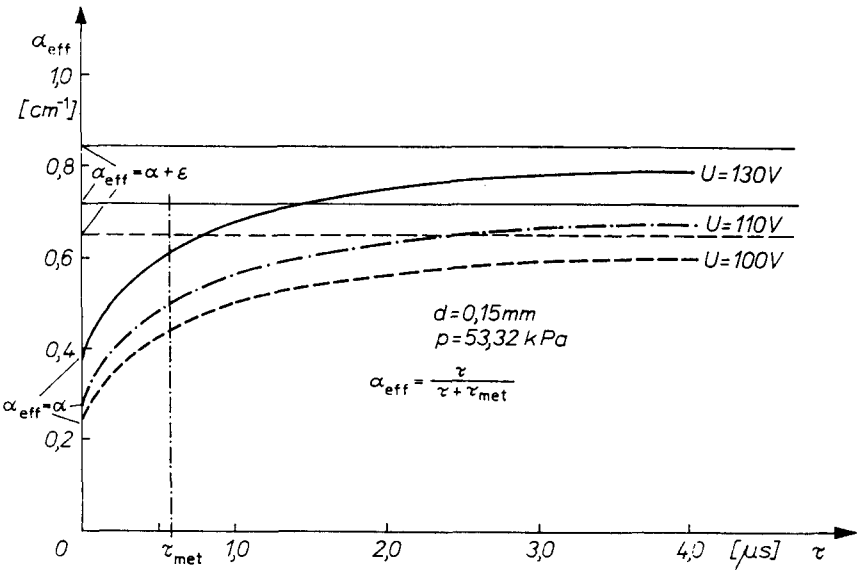

Fig. 16: Dependence of the effective Townsend ionization coefficient α_{eff} on the characteristic time τ, Parameter: U

Fig. 16 shows the dependence of the effective Townsend ionization coefficient α_{eff} on the characteristic time τ for different discharge voltages. Therefore the characteristic time τ is the main factor determining the proportion of metastable Ne atoms involved in ionization. The limit for $\tau \to o$ is the well known 1st Townsend ionization coefficient α, i.e. ionization takes place by electron collisions, ionization by metastable neon atoms is negligible. For $\tau \to \infty$ the metastable neon atoms are those predominantly involved in

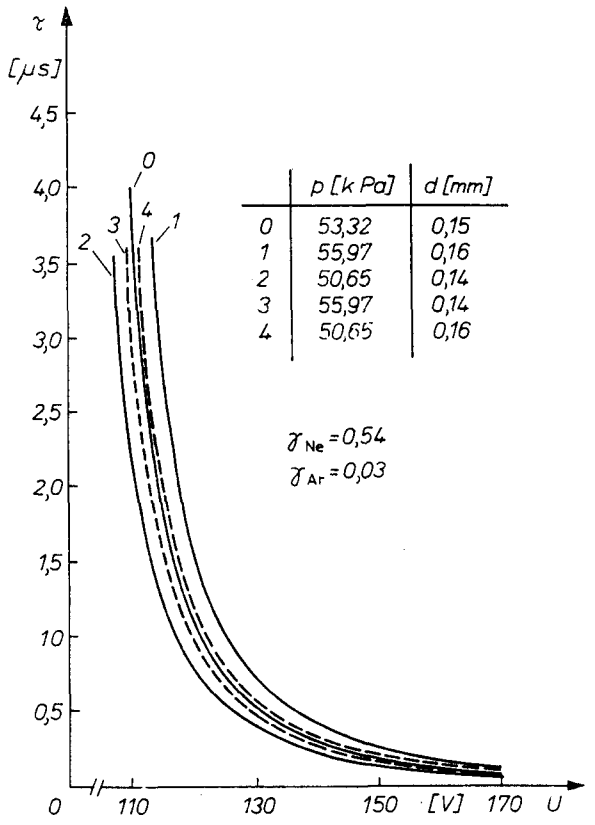

Fig. 17: Calculated results as to the dependence of the characteristic time on the discharge voltage, Parameter: p, d

ionization (for these discharge conditions ε exceeds α about the factor 3). Interesting is just the transition region of τ, there is a shift from pure electron collision ionization to ionization processes essentially determined by metastables. (Lifetime of metastable neon atoms τ_{met} is also shown.)

Fig. 17 shows calculated results as to the dependence of the characteristic time on the discharge voltage. As secondary emission coefficients values from the literature are used ($\gamma^0_{Ne} = 0.54$, $\gamma^0_{Ar} = 0.03$) [35], and the backscattering of electrons at the cathode is taken into account [15]. The parameters are pressure p and gas space thickness d. The family of curves illustrates the effects of relatively small differences in gas pressure and plate distance on the physical behaviour of display discharges.

Fig. 18 shows the comparison of measured values to the characteristic time τ with calculated curves in dependence on the discharge voltage. The measurements refer to two different discharge cells of a plasma display of 90×90 discharge cells (PAF 90, $p = 53.32$ kPa, $d = 0.16$ mm) and to a PAF 128 discharge cell. The experimental values are easy to approximate by calculated functions. The secondary emission coefficients of the discharge cell cathode for neon and argon ions, respectively, are the material constants. They characterize the properties of the MgO layer. γ^{Ne} and γ^{Ar} are varied until adaptation between measurement and calculation is achieved.

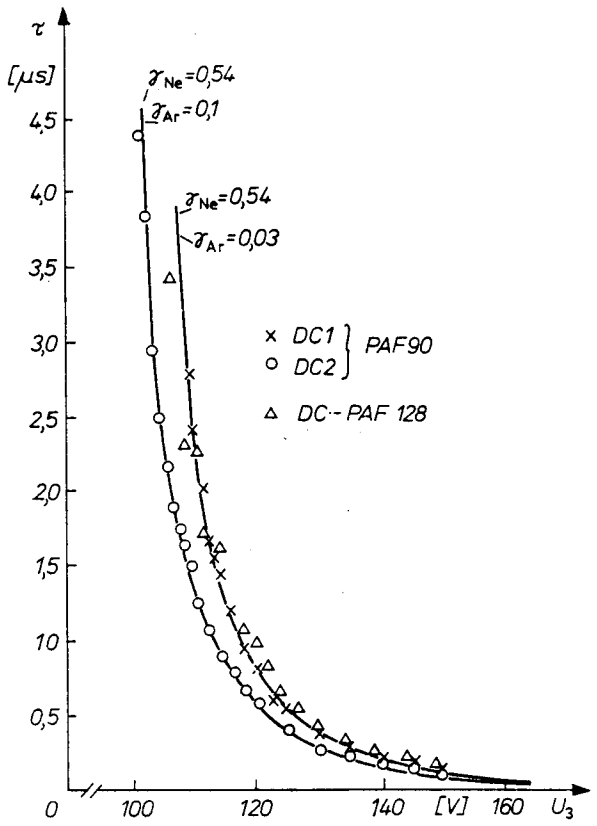

Fig. 18: Comparison of measured values to the characteristic time τ with calculated curves in dependence on the measuring pulse voltage
Parameters: γ^{Ne}, γ^{Ar}, — PAF 90/128 —

Fig. 19 shows an analogous result for two PAF 58 discharge cells. Also here the measured values can easily be approximated by calculated functions. However, the calculations yield essentially decreased secondary emission coefficients γ^{Ne}, γ^{Ar} in comparison to PAF 90, which suggests quantitative differences in the physical properties between the MgO layer of PAF 58 and that of PAF 90. The reason for the increased range of measured values of PAF 58 has already been mentioned above (see also [24]). The theoretically excepted linear relationship between characteristic time and build-up time in the investigated parameter ranges could be confirmed by the experiments (Fig. 15).

A prerequisite for comparing measurements of the characteristic time of dispaly discharges with calculated values is the knowledge of the wall voltage conditions in the

discharge cell prior to the measuring pulse. Due to the method of minimizing the wall voltage by a siutable erase pulse described in Sec. 4, the measuring pulse voltage U_3 is equal to cell voltage. Thus an immediate comparison of calculated values with experimental results is possible.

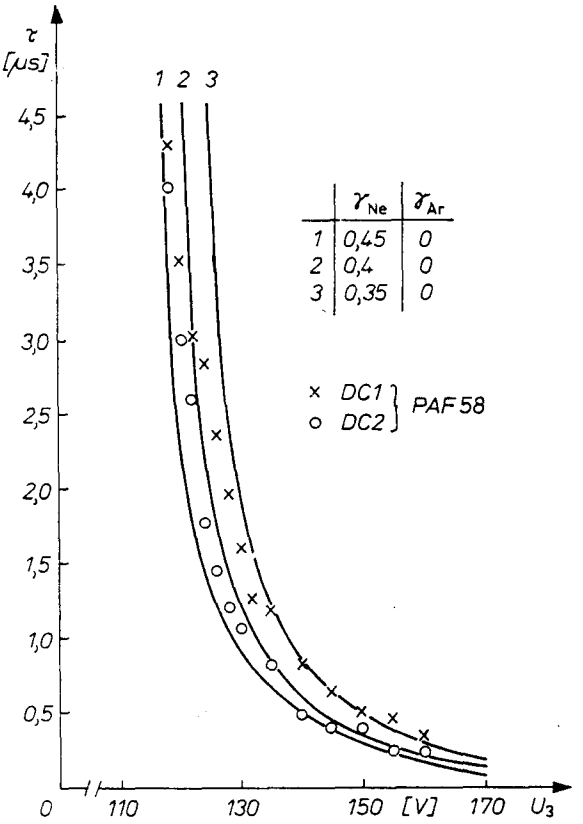

Fig. 19: Comparison of measured values to the characteristic time with calculated curves in dependence on the measuring pulse voltage
Parameters: γ^{Ne}, γ^{Ar}, — PAF 58 —

References

[1] Slottow, H. G., Petty, W. D., Coord. Sci. Lab., Univ. Illinois, Report R-497 (1970).
[2] Müller, S., Dissertation, Greifswald 1980.
[3] Slottow, H. G., IEEE Trans. on Electr. Dev. ED-24 (1977) 848.
[4] Weber, L. F., Dissertation. Illinois 1975.
[5] Bartholomeyczyk, W., Zeitschrift für Physik **116** (1940) 235.
[6] V. Gugelberg, H. L., Helv. Phys. Acta **20** (1947) 308.
[7] Makranczi, B., Acta Phys. Acad. Sci. Hung. **28** (1970) 279.
[8] Fucks, W., Archiv f. Elektrotechnik XL (1950), 1.
[9] Boiziau, C., Scanning Electron Microscopy III (1982) 949.
[10] Hagstrum, H. D., Phys. Rev. **50** (1966) 495.
[11] Le Gressus, L., Vigouroux, J. P., Duraud, J. P., et al., Scanning Electron Microscopy I (1984) 41.

[12] VIGOUROUX, J. P., DURAUD, J. P., LE MOEL, A., et al., Nucl. Instr. and Meth. in Phys. Res. **B1** (1984) 521.
[13] VIGOUROUX, J. P., DURAUD, J. P., LE MOEL, A., et al., J. Appl. Phys. **57** (1985) 5139.
[14] VIGOUROUX, J. P., LE GRESSUS, C., DURAUD, J. P., Scanning Electron Microscopy **II** (1985) 513.
[15] SAHNI, O., LANZA, L., HOWARD, W. E., J. Appl. Phys. **49** (1978) 2365.
[16] VERON, H., WANG, C. C., J. Appl. Phys. **43** (1972) 2664.
[17] UCHIKE, H., ANDOH, S., MURASE, K., et al., Trans. IECE 81/11 vol. J. 64 — C, 793.
[18] NIGHAN, W. L., IEEE Trans. on Electr. Dev. ED-**28** (1981) 625.
[19] ABOELFOTOH, M. O., LORENZEN, J. A., J. Appl. Phys. **48** (1977) 4754.
[20] ABOELFOTOH, M. O., SAHNI, O., IEEE Trans. on Electr. Dev. ED-**28** (1981) 645.
[21] SAHNI, O., ABOELFOTOH, M. O., IEEE Trans. on Electr. Dev. ED-**28** (1981) 638.
[22] ABOELFOTOH, M. O., SAHNI, O., IBM Techn. Discl. Bull. **24** (1981) 1 B ,557.
[23] ABOELFOTOH, M. O., IBM Techn. Discl. Bull. **25** (1982) 3 D, 1530.
[24] ANDOH, S., MURASE, K., UMEDA, S., et al., IEEE Trans. on Electr. Dev. ED-**23** (1976) 319.
[25] ZAHN, R.-J., MÜLLER, S., Beitr. Plasmaphys. **19** (1979) 107.
[26] NASTASE, L. E., LUNGU, C. P., OANCEA, A. M., et al., 16th ICPIG, Düsseldorf 1983, 576
[27] ACTON, J. R., SWIFT, J. D., Cold Cathode Discharge Tubes, Heywood London 1963.
[28] STERN, W., HOLTZ, P., Lab.-Bericht 38 (1982), ZIE V.
[29] WEBER, L. F., IEEE Trans. on Electr. Dev. ED-**24** (1977) 859.
[30] SCHADE, R., Zs. f. Phys. **104** (1937) 489.
[31] ROGOWSKI, W., Zs. f. Phys. **115** (1940) 257.
[32] STEENBECK, M., Wiss. Veröff. d. Siemens-Konzerns **9** (1930) 42.
[33] GÄNGER, D., Der elektrische Durchschlag in Gasen, Springer Verlag Berlin, Heidelberg, New York 1957.
[34] BITZER, D. L., SLOTTOW, H. G., WILLSON, R. H., Coord. Sci. Lab., Univ. Illinois, Quarterly Process Report 31, Sept.—Nov. 1964.
[35] ABOELFOTOH, M. O., IEEE Trans. on Electr. Dev. ED-**29** (1982) 247.

Received May 22, 1987